IEEE Access
Multidisciplinary | Rapid Review | Open Access Journal

Received 25 October 2022, accepted 1 December 2022, date of publication 12 December 2022,
date of current version 20 December 2022.

Digital Object Identifier 10.1109/ACCESS.2022.3228764

RESEARCH ARTICLE

3D-Printed Dielectric Resonators for Quasi-TE112 Mode Singlets, Doublets and Dual-Mode Filters

LUKE ROBINS[1], (Member, IEEE), CHAD BARTLETT[2], (Graduate Student Member, IEEE), ARASH ARSANJANI[1], (Member, IEEE), ABDULRAHMAN WIDAA[2], (Graduate Student Member, IEEE), REINHARD TESCHL[1], (Member, IEEE), MICHAEL HÖFT[2], (Senior Member, IEEE), AND WOLFGANG BÖSCH[1], (Fellow, IEEE)

[1]Institute of Microwave and Photonic Engineering, Graz University of Technology, 8010 Graz, Austria
[2]Department of Electrical and Information Engineering, Kiel University, 24143 Kiel, Germany

Corresponding author: Luke Robins (lrobins@tugraz.at)

This work was supported by the European Union's Horizon 2020 Research and Innovation Programme under the Marie Skłodowska-Curie Grant 811232-H2020-MSCA-ITN-2018.

ABSTRACT This paper demonstrates the use of a ceramic stereolithography-based additive manufacturing process to fabricate higher-order mode dielectric resonators. In this work, dielectric resonators with concentric rings around a combline rod structure are 3D-printed using alumina. The integration of the concentric rings for the use of the TE_{112} mode allows for a more compact cavity structure and a higher unloaded quality factor when compared to a simple dielectric combline resonator with a similar S-parameter response. The achievable improvements in quality factor for the TE_{112}-mode resonators utilising concentric rings are compared through simulations and experimental results. The measured results demonstrate an increased average in the unloaded quality factor of $Q_u \approx 2172$ which is approximately 44%. Additionally, the application of the 3D-printed resonators is further demonstrated in a TE_{112} singlet, doublet, and dual-mode filter configuration.

INDEX TERMS Additive manufacturing, bandpass filter, dielectric resonator, doublet, dual-mode, miniaturisation, passive components, singlet, stereolithography.

I. INTRODUCTION

Radio frequency (RF) filters are critical building blocks of modern telecommunication systems for terrestrial and satellite applications. In a typical RF receiver, for example, the placement of a filter directly after the receiving antenna means that the filter's performance significantly contributes to the overall system loss, noise, and power handling performance. The higher the insertion loss of the filter, the higher its contribution to the noise figure, with higher thermal expansion/heat, and lower overall achievable throughput [1], [2].

Specifically for space applications, more losses in the system mean more resources or costs need to be provisioned for thermal management systems or means of heat dissipation. These factors highlight the necessity to optimise the return loss (RL) and quality factor of the required filters. For that reason, architectures that are known for high quality factors like microwave cavities and dielectric resonators have widely been used in satellite communication systems [3], [4], [5], and in addition, several different approaches to improving the quality factor of these types of filters are extensively described in the literature [6], [7], [8], [9], [10], [11], [12], [13], [14], [15], [16].

In the case of coaxial combline resonators, periodic rings have been used to achieve a virtual enlargement of the resonator, i.e. increasing the inductance [6]. The work presented in [7] demonstrates a reduction of the ohmic losses with minimal added manufacturing complexity by rounding the corners in the cavity and bottom of the coaxial resonator. Nevertheless, the achievable quality factor of such metallic coaxial structures still does not

The associate editor coordinating the review of this manuscript and approving it for publication was Wenjie Feng.

meet the stringent requirements for several high-performance applications.

A standard approach to achieving increased quality factor performance in cavities is using dielectric resonators to concentrate the fields away from the walls of the housing cavity, thus reducing the losses and increasing quality factor [8], [9]. As an alternative to the $TE_{01\delta}$ mode traditionally utilised in the literature, reference [10] demonstrates three-layered TE_{102} mode Bragg-reflection dielectric resonators, which achieve quality factors one order of magnitude higher than conventional resonators. Another design in [11] makes use of a dielectric post that has been shaped in such a way to make mounting in the middle of a cavity possible, thus moving the fields away from the floor and roof of the resonator and reducing losses when compared to a similar TM or combline dielectric resonator configuration.

Besides low-loss (and associated high quality factor), the need for simplified assembly and size reduction is usually also a requirement that drives innovation, most notably in weight and power sensitive application areas like satellite communications. The combination of additive manufacturing with dielectric materials provides the opportunity to tackle these requirements simultaneously. In [12], the authors demonstrate how the use of a novel additively-manufactured alumina resonator can be used to enable this in filter applications. Another example is the approach of manufacturing ceramic monoblock filters, which has received a lot of interest as it requires in the ideal case only metallisation and minimal assembly. Examples of various TM single and dual-mode printed filters are provided in [13], [14], and [15]. Metallisation and manufacturing tolerances proved challenging in [13] and [14]. In reference [15], more success was achieved by including a metal mask/backplate on which the tuning elements could be attached so that the manufacturing defects could be more easily compensated. In [16], the ability to print variable dielectric constants inside waveguide structures to achieve bandpass filtering was proposed.

The work in this paper demonstrates how the flexibility of additive manufacturing (AM) can be used to increase quality factor performance through changes in the geometry of a dielectric resonator. To this end, the concept of periodic perturbations in the form of concentric rings around a dielectric resonator rod is explored to improve the quality factor performance of filters and resonators. The remainder of the paper is split into five sections; first, the effect of geometric variations in the form of concentric rings on a post resonator is demonstrated to improve the obtainable quality factor. The proposed resonator is then implemented into a singlet configuration in a metallic cavity where examples of transmission-zero control are highlighted. Subsequently, the performance of the novel singlet configuration is compared to an equivalent singlet with a standard ceramic-rod resonator. The configuration is later expanded into a doublet configuration, which was fabricated and measured, to demonstrate the potential applications of the proposed structure. Lastly, a dual-mode four-pole filter is demonstrated and discussed with the results then briefly concluded.

II. CONCENTRIC-RING RESONATOR DESIGN

The effect of adding concentric rings on a metallic combline resonator to increase the quality factor was demonstrated in [6], through the use of a metallic combline/ring structure. Simulation of the quality factor showed an improvement in the order of $Q_l \approx 200$ for the addition of three concentric rings, and $Q_l \approx 400$ for six concentric rings. In this work, a similar approach is studied using sets of concentric rings on dielectric combline resonators to provide compactness and improve quality factor performance.

A. CAVITY MODES

To study the effects of concentric rings placed around dielectric posts, first, the resonate modes of the simple post were simulated and identified for reference. An alumina ($\varepsilon_r = 9.5$) post with a length of 18.6 mm and a diameter of 4.61 mm, positioned inside a cylindrical cavity (height of 21.95 mm, diameter of 12 mm) with one end grounded, illustrated in Fig. 1.(a), has a quasi TM_{010} electromagnetic field as the fundamental mode at approximately 8.9 GHz.

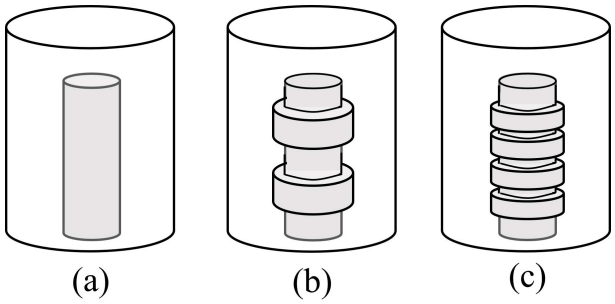

FIGURE 1. Dielectric combline post resonator with (a) no rings, (b) two concentric rings, and (c) four concentric rings.

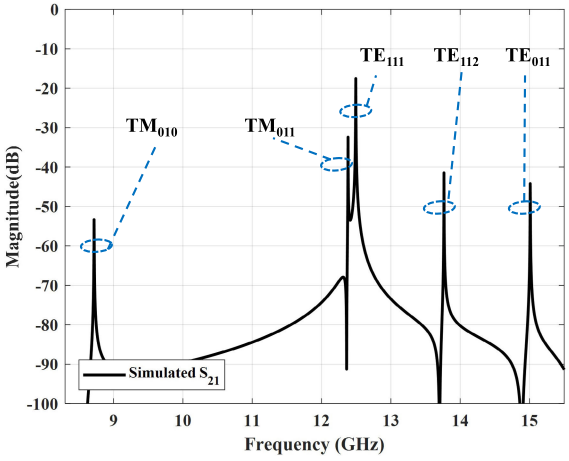

FIGURE 2. Weakly excited quasi-TM cylindrical dielectric combline cavity modes.

The fields due to the resonator being positioned on the floor of the cavity, are not identical to a pure TM_{010} mode

as they have components in the propagation direction, and the maxima of the fields are shifted in position. The contribution of the field in the Z-direction is significantly smaller. Thus, considering the pure mode provides insight into the behaviour of the resonator and enables design or excitation choices. This quasi-mode behaviour applies to the rest of the modes discussed as well. The resonator was simulated with a weak excitation, the response of which is shown in Fig. 2. These modes were identified to be the (1) TM_{010}, (2) TM_{011}, (3 & 4) TE_{111}, (5 & 6) TE_{112} and (7) TE_{011}, with simplified field representations shown in Fig. 3. Note that the TE_{111} and TE_{112} modes have identical orthogonal modes at their resonant frequencies, which can be used in dual-mode configurations.

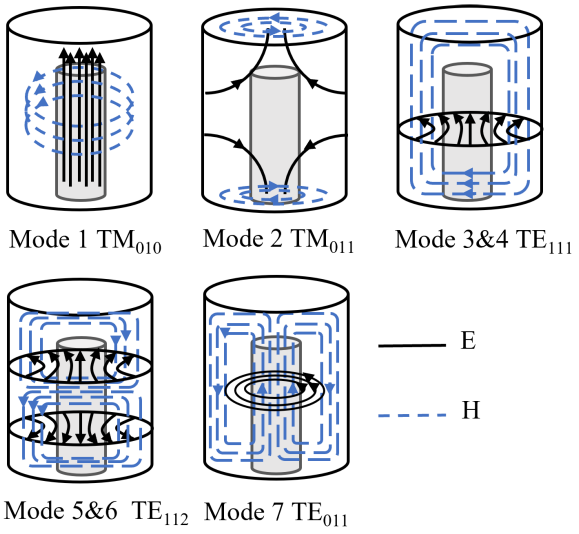

FIGURE 3. Quasi-TM cylindrical dielectric combline cavity modes.

B. APPLICATION OF CONCENTRIC RINGS

Adding rings to the simple post resonator in symmetrical pairs increasing in number as illustrated in Fig. 1 was investigated. The number of rings, as well as their size and spacing affect the structure's quality factor performance. Additionally, the changes will shift the resonator's centre frequency, so this needs to be compensated for to ensure performance at the desired frequency. Applying symmetrical pairs of rings onto the post was found to have an increase in quality factor for the TE_{112} mode, with the quality factor of lower modes remaining largely the same as that of the simple post.

In order to obtain an optimal quality factor, the fields should be moved upwards, away from the floor of the cavity. When positioned correctly, the rings provide a similar effect to the solution proposed in [11], which reduces the losses due to the currents in the bottom wall of the cavity which in turn raises the quality factor. The unloaded quality factor is proportional to the energy stored by the resonator over the energy dissipated as described in Equation (1). The elements contributing to the loss in these configurations are dominated by the conductor losses and the dielectric losses as shown in Equation (2). As the alumina used has a very low loss of $\tan\delta = 8{\cdot}10^{-5}$ [17], reducing the conductor losses will have the greatest impact on the quality factor. This can be achieved by raising the conductivity of the sidewall material or moving the field away from the walls. Fig. 4 and Fig. 5 show the effect of using zero, two and six concentric rings on the electric and magnetic fields, which are gradually being moved to the centre of the cavity. Table 1 and Fig. 6 demonstrate a comparison of the quality factor of the resonator with varying symmetrical concentric-ring configurations inside brass and copper cavities. At 14 GHz, an increase of around 2700 was achieved for the TE_{112} mode using six rings when compared to that of the post.

$$Q_u \propto \frac{E_{stored}}{E_{dissipated}} \tag{1}$$

$$\frac{1}{Q_u} = \frac{1}{Q_c} + \frac{1}{Q_d} \tag{2}$$

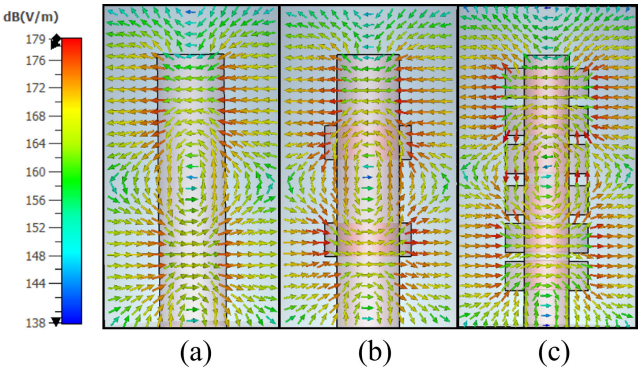

FIGURE 4. E-field comparison of (a) post, (b) two and (c) six concentric-ring resonators.

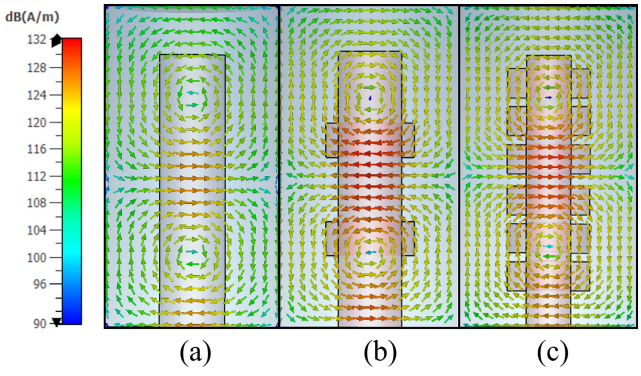

FIGURE 5. H-field comparison of (a) post, (b) two and (c) six concentric-ring resonators.

III. 3D-PRINTING METHODOLOGY AND CONSIDERATIONS

The printing process, technology, and materials used in ceramic-based additive manufacturing lead to considerations

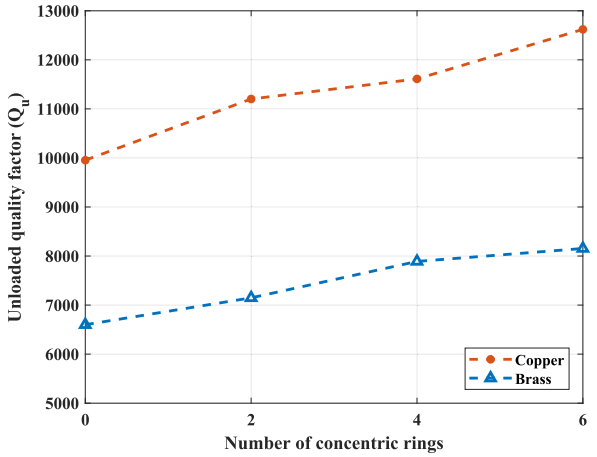

FIGURE 6. Quality factor comparison for CW614N brass and CW008A copper alloys with varying concentric-ring configurations.

TABLE 1. Number of concentric rings with an estimated quality factor with a constant volume of $0.28{\cdot}\pi \cdot \lambda_0^3$ at 14 GHz (where λ_0 is wavelength at the centre frequency).

Number of concentric rings	None	Two	Four	Six
Q_u CW614N brass	6600	7148	7890	8154
Q_u CW008A copper	9954	11202	11611	12621

that must be factored in at the design stage. The technology used for the printing of the alumina resonators is known as lithography-based ceramic manufacturing (LCM) [18]. The 3D-print process flow is shown in Fig. 7, which starts with the preparation of a CAD model (1). The material, in this case Lithalox HP350, is a printable slurry consisting of powdered ceramic particles that are suspended in a photosensitive organic binder (2). The slurry is hardened layer by layer onto a build platform using ultraviolet light (3). Next, the printed parts need to be cleaned using airbrushes and a solvent, as they are covered in uncured slurry resulting from the printing, which needs to be removed (4). Once complete, the parts must undergo a debinding step to remove the organic binder (5), followed by a sintering step (6) to form dense ceramic parts. The debinding and sintering steps are done at high temperatures up to 1650 °C and shrinkage of the parts occurs, which needs to be compensated for at the print step. The values of shrinkage compensation used for the HP350 were taken as 1.233 in XY- and 1.273 in Z- direction [15]. Depending on the geometry, these values may need to be adjusted slightly for more accuracy, once the final part dimensions are measured. The CeraFab 7500 printer was used, with an XY resolution of 40 μm and printing-layer height of 50 μm.

A centre frequency of 14 GHz was chosen to be within a printable range of sizes with the given dielectric constant. The large diameter difference between the rings and the central post creates shear stress failure points, which can delaminate during the printing process. Large unsupported overhangs are also prone to sagging under their own weight. To avoid these issues, a chamfer was added to the bottom edge of each of the rings in order to provide a more gradual transition. The modification caused a reduction of around 550 in the quality factor, as the rings had to be made thicker and could not be positioned as closely together. The printed resonator dimensions are given in Fig. 8 with the printed resonators shown in Fig. 9 during the cleaning procedure.

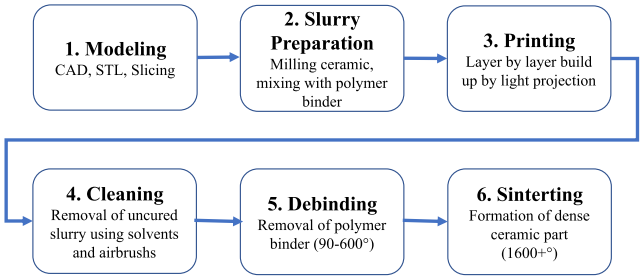

FIGURE 7. Ceramic 3D-print process flow.

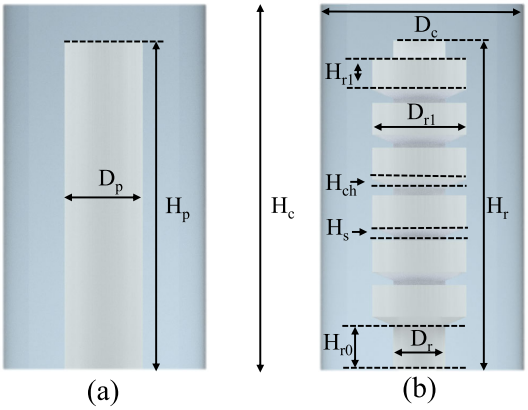

FIGURE 8. (a) Simple post dimensions: $D_p = 4.61$, $H_p = 18.6$ and (b) concentric-ring resonator with dimensions: $H_{r0} = 2.5$, $H_{r1} = 1.8$, $D_c = 12$, $H_c = 18.83$, $D_r = 3.07$, $D_{r1} = 5.55$, $H_s = 0.733$, $H_{ch} = 0.5$ (all dimensions are given in mm).

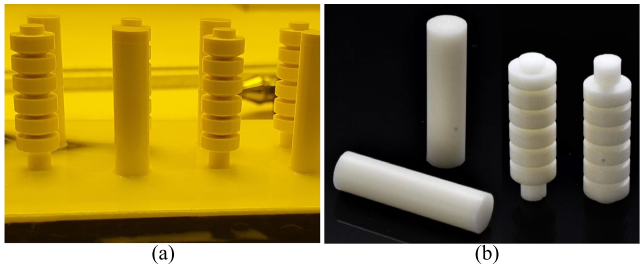

FIGURE 9. Printed alumina post and concentric-ring resonators (a) during cleaning and (b) after debinding and sintering process.

IV. DESIGN AND SIMULATION

In this section, the design parameters and simulated performances of the singlet, doublet, single-mode and dual-mode filters are discussed.

A. TE_{112} MODE SINGLET

A single resonator with input and output ports can be set up to achieve a pole and transmission zero combination by exciting one of the TE_{112} modes with a TE_{111} source-to-load bypass coupling. This type of structure can be described by a singlet configuration which has been extensively detailed in work such as [19], and [20]. The positioning of the transmission zero can be influenced by moving the position of the probe feeds along the height of the resonator. The phase relationship between the TE_{112} and the TE_{111} at the two ports can be exploited to shift the position of the transmission zero below or above the passband. Fig. 10 demonstrates the possible port configurations (inline or offset). If the fields of both modes at the ports are in phase with each other, the transmission zero will be positioned below the passband, and if the modes at the ports are out of phase at either port, the transmission zero will appear above the passband, as demonstrated in detail in [21] and [22]. Fig. 11 and Fig. 12 demonstrate possible transmission zero configurations for below and above the passband, respectively. The transmission zeros can be positioned freely all the way to the lower and upper spurious bands. The depth

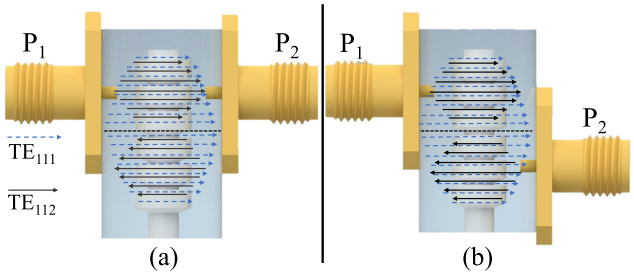

FIGURE 10. Singlet port configurations highlighting the (a) in-phase and (b) out of phase TE_{112} and bypass TE_{111} respectively.

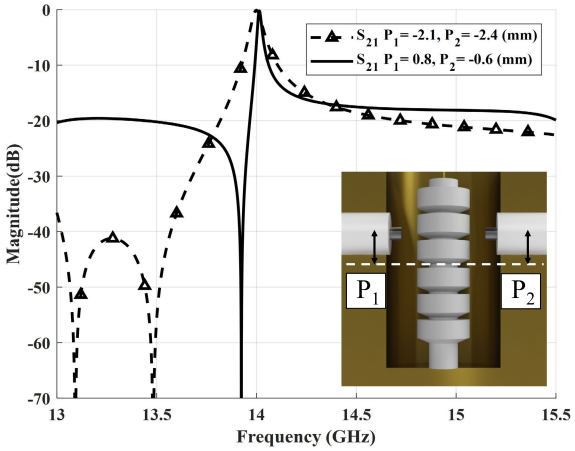

FIGURE 11. Simulated singlet left-hand transmission zero configurations with dimensions: dashed $P_1 = -2.1$, $P_2 = -2.4$, $C_h = 21.5$, $P_L = 1.2$ and solid $P_1 = 0.8$, $P_2 = -0.6$, $C_h = 21.7$, $P_L = 1.3$ (all dimensions are given in mm).

and height of the probe feed influence the input coupling as shown in Fig. 13. If finer control and stronger input coupling are required, the probe can be replaced with a T-shaped feed

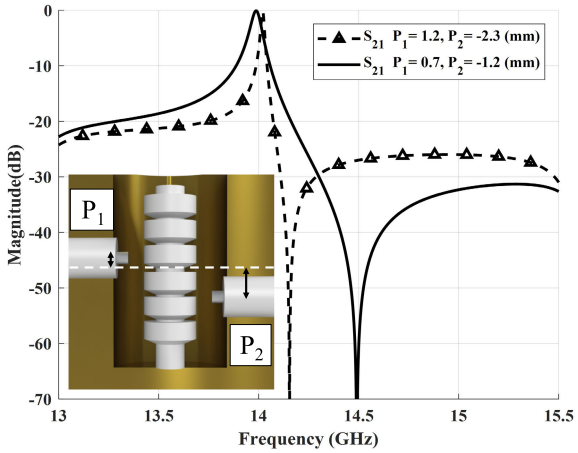

FIGURE 12. Simulated singlet right-hand transmission zero configurations with dimensions: dashed $P_1 = 1.2$, $P_2 = -2.3$, $C_h = 21.7$, $P_L = 1.1$ and solid $P_1 = 0.7$, $P_2 = -1.2$, $C_h = 21.7$, $P_L = 1.1$ (all dimensions are given in mm).

structure, shown in Fig. 14, by soldering a piece of wire to the end of the probe. A comparison of the achievable input coupling of the probe compared to the T feed for the same heights is shown in Fig. 14. This comes at the cost of increased assembly complexity and modification difficulty. The width of the wire attached to the pin also influences coupling strength, resonant frequency and achievable transmission zero positions, all of which need to be considered when using this type of feeding.

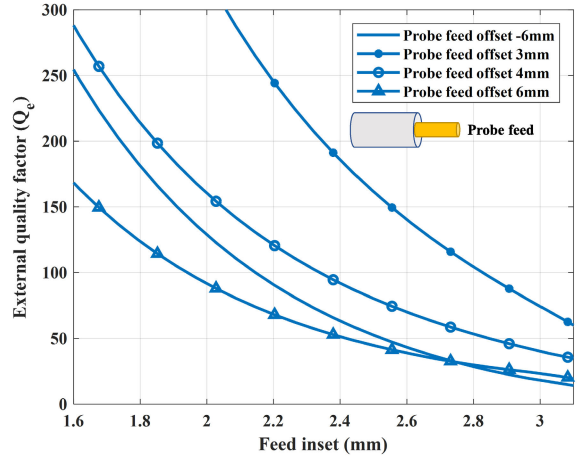

FIGURE 13. Input coupling for varying feed heights and inset depths.

A cylindrical cavity was chosen for this implementation to provide the ability to rotate the feeds and the coupling screws around the cavity in the upcoming dual-mode configuration. A singlet was designed for the standard post case as well as for the concentric-ring resonator. The pole/zero locations were optimised for both cases to have a similar response. The coupling matrix of the singlets is given in Equation (3).

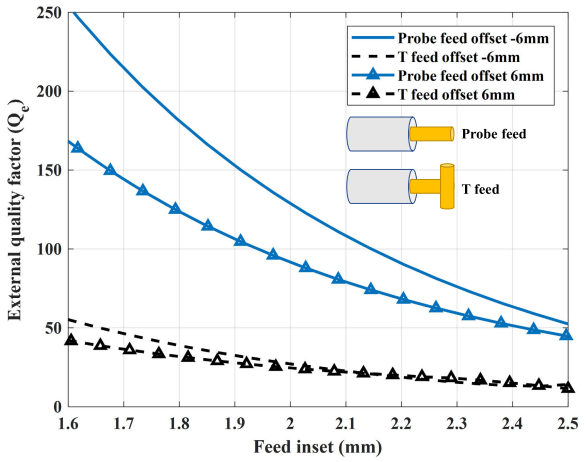

FIGURE 14. Input coupling probe feed vs T feed for varying feed heights and inset depths.

Fig. 15 shows the simulated performance of both singlets.

$$M = \begin{bmatrix} 0 & 2.23 & -0.04 \\ 2.23 & 0.41 & 2.23 \\ -0.04 & 2.23 & 0 \end{bmatrix} \quad (3)$$

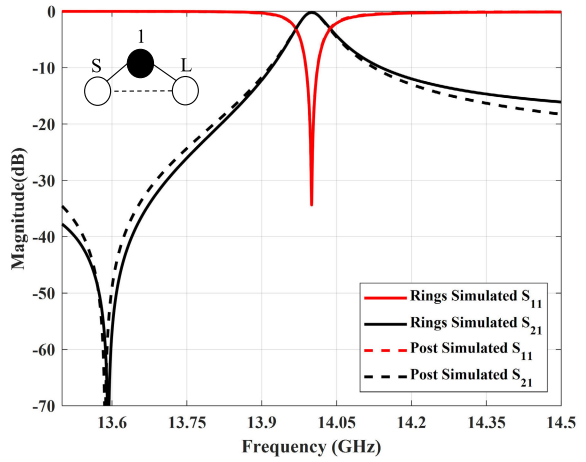

FIGURE 15. Simulated concentric-ring singlet with dimensions: $P_1 = P_2 = -2.085$, $C_h = 21.4$, $P_L = 2.1$ compared to post singlet with dimensions: $P_1 = P_2 = -4.26$, $C_h = 21.95$, $P_L = 2.4$ (all dimensions are given in mm).

B. TE_{112} DUAL-MODE DOUBLET

Using both orthogonal TE_{112} modes, a doublet [23], [24] can be implemented in a single cavity. The dual-mode operation is achieved using a screw at 45° to excite both modes within the cavity. Two additional screws are used to control the centre frequency of each of the poles in much the same way as the method described for the TE_{111} mode in [25] and [26]. Fig. 16 shows the strength of coupling of the two modes based on the depth of the screw. The deeper the screw, the stronger the coupling into the second TE_{112} mode. It is also important to note that the position of the screw along the resonator influences the maximum achievable coupling strength. The screws should be placed at the maximum of the fields for the strongest effect. The position can be changed depending on the desired coupling to optimise for the manufacturing process, however, they also have an effect on the transmission zero positioning, which needs to be compensated. The second feed was rotated around the axis of the resonator by $\theta = 52°$ to shift the second transmission zero above the passband as shown in the inset of Fig. 17. The coupling matrix of the doublet is given in Equation (4). Fig. 17 shows the simulated response of an exemplary doublet configuration. The transmission zero positions are more limited in the doublet configuration as it is difficult to move the transmission zeros independently and separately from the pole positions.

$$M = \begin{bmatrix} 0 & 0.69 & -0.98 & 0.07 \\ 0.69 & -1.64 & 0 & 0.69 \\ -0.98 & 0 & 1.612 & 0.98 \\ 0.07 & 0.69 & 0.98 & 0 \end{bmatrix} \quad (4)$$

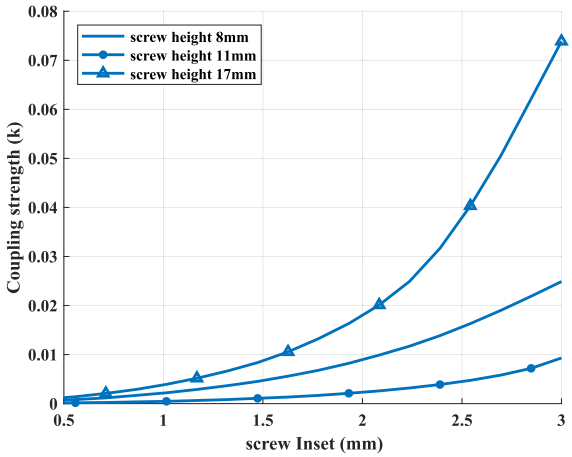

FIGURE 16. Dual-mode coupling with screw depth for various heights along the cavity.

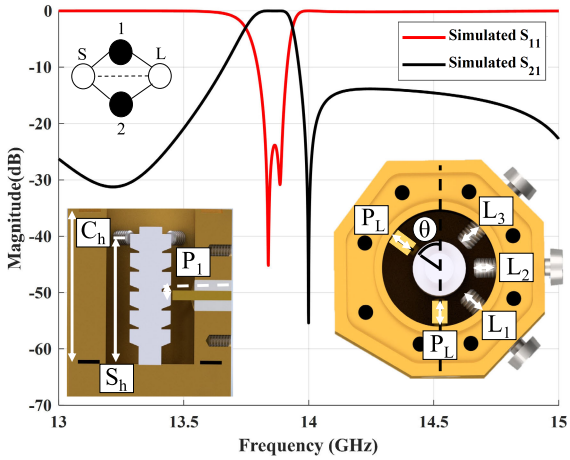

FIGURE 17. Simulated doublet with dimensions: $P_1 = P_2 = -1.16$, $C_h = 20.95$, $S_h = 18$, $P_L = 3.15$, $L_1 = 1.85$, $L_2 = 1.9$, $L_3 = 0.75$ and $\theta = 52°$ (all dimensions are given in mm).

C. CASCADED SINGLETS

Two singlets were positioned back to back, with a coupling iris, to achieve a two-pole filter for demonstration purposes.

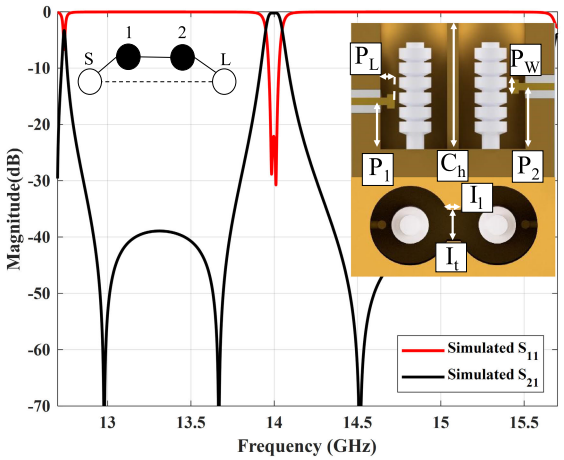

FIGURE 18. Simulated single mode filter with dimensions: $P_1 = 8.37$, $P_2 = 12.86$, $C_h = 22.48$, $P_L = 1.87$, $P_W = 2.5$, $I_t = 4.75$, and $I_l = 0.5$ (all dimensions are given in mm).

A T-shaped feed was chosen to enable stronger input coupling as demonstrated in Fig. 14. The transmission zeros of the filter are achieved in the same way as for the individual singlet, where the position of the feeds along the height of the resonator determines their location. The transmission zeros were positioned close to the passband to achieve a steep cutoff, with the filter centred at 14 GHz and a fractional bandwidth of 0.3%. The coupling matrix is given in Equation (5), and the simulated performance of the filter is given in Fig. 18.

$$M = \begin{bmatrix} 0 & 1.22 & 0 & -0.0062 \\ 1.22 & 0 & 1.658 & 0 \\ 0 & 1.658 & 0 & 1.22 \\ -0.0062 & 0 & 1.22 & 0 \end{bmatrix} \quad (5)$$

D. TE_{112} DUAL-MODE FOURTH-ORDER FILTER

The doublet can also be extended into a back-to-back configuration to create a four-pole, two-zero, dual-mode filter. The coupling between the two resonators is achieved through a split iris, separated by a solid block in the centre. This block allows the TE_{112} mode to couple while rejecting most of the TM_{011} mode and pushing the TE_{112} mode to lower frequencies, thus increasing the spurious free range below the passband by approximately 1.5 GHz. A comparison between this design and a standard iris can be seen in the inset of Fig. 19, where a demonstration of the improved spurious performance is depicted. The coupling matrix of the dual-mode filter is given in Equation (6), while Fig. 20 shows the simulated performance of such a dual-mode configuration centred at 14 GHz and a fractional bandwidth of approximately 1.3%.

$$M = \begin{bmatrix} 0 & 1.03 & 0.145 & 0 & 0 & 0 \\ 1.03 & -0.25 & 0.9 & 0 & 0 & 0 \\ 0.145 & 0.9 & 0.11 & 0.7 & 0 & 0 \\ 0 & 0 & 0.7 & -0.05 & 0.9 & -0.08 \\ 0 & 0 & 0 & 0.9 & 0.15 & 1.03 \\ 0 & 0 & 0 & -0.08 & 1.03 & 0 \end{bmatrix} \quad (6)$$

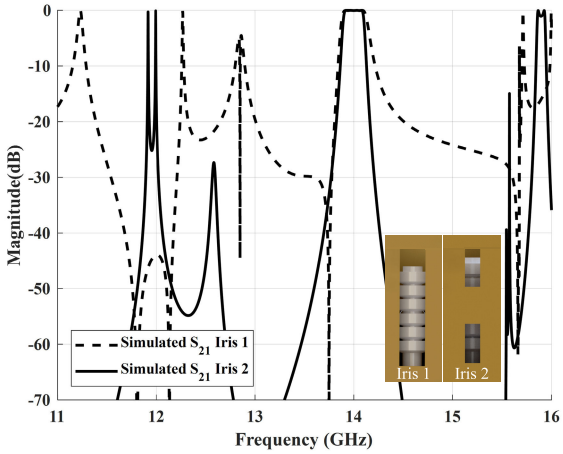

FIGURE 19. Iris comparative response of full height Iris 1 and centre block TM_{011} rejection Iris 2.

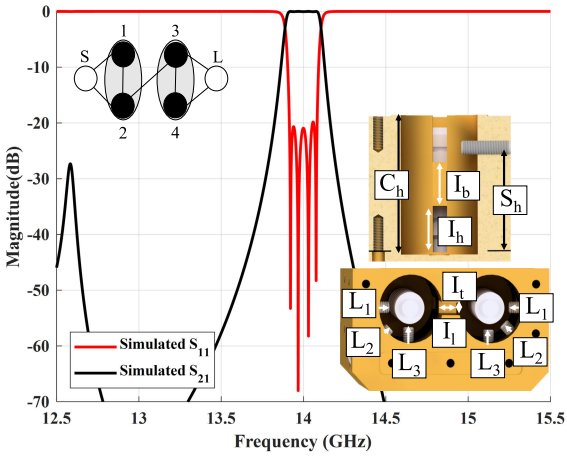

FIGURE 20. Simulated dual-mode filter with dimensions: $C_h = 20.7$, $P_L = 3.12$, $I_h = 6.74$, $I_b = 6.36$, $S_h = 15.5$, $I_t = 2.23$, $I_l = 3.3$, $L_1 = 0.85$, $L_2 = 1.44$ and $L_3 = 1.26$ (all dimensions are given in mm).

V. MEASUREMENT DISCUSSION

In this section, the measurement results of the fabricated singlets, doublet and dual-mode filters are discussed. After fabrication, the dielectric resonators were found to be slightly larger than specified due to over-polymerisation of approximately 60 μm on each side in the XY-direction. As Fig. 21 illustrates, changes in the outside diameter of the resonator lead to a shifting of the resonant frequency. The over-polymerisation caused a 2.16% increase in the dimensions of the resonators and led to a downward shift in frequency of approximately 173 MHz in a simplified eigenmode simulation. Secondly, glueing the resonators to the floor of the cavities, thereby removing direct contact with the metal by inserting a lower dielectric material layer between the two, also shifts the resonant frequency downwards. Misalignment and tilting of the resonators during the manual assembly can lead to additional frequency shifts, especially of the transmission-zero positions. These effects will be demonstrated in the doublet and dual-mode filter cases by inclusion into a modified simulation model to validate.

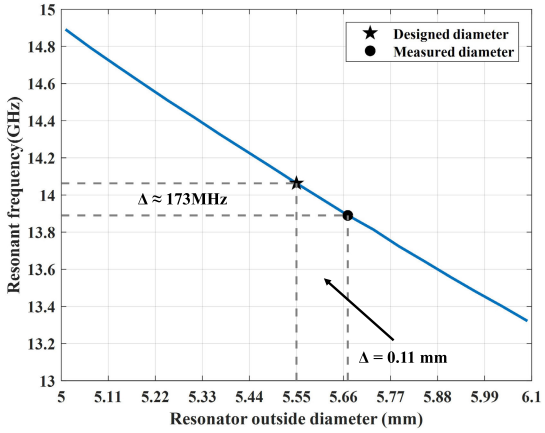

FIGURE 21. Concentric ring resonator outside diameter vs TE_{112} mode resonant frequency.

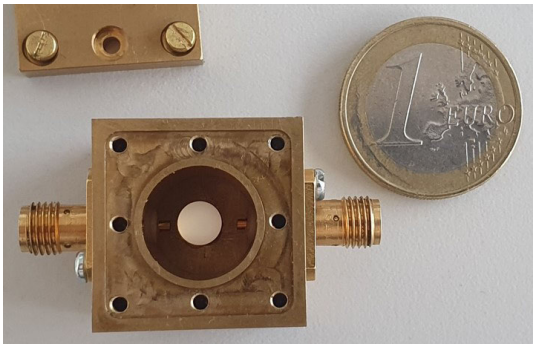

FIGURE 22. Fabricated TE_{112} mode post resonator singlet.

A. QUALITY FACTOR

Two sets of cavities were milled for the printed resonators, one of each made from CW614N brass and CW008A copper alloys with electrical conductivities of 14.6 MS/m and 58 MS/m as per the data-sheet [29] and [30], respectively. The resonators were then glued to the base of the lid in each cavity as shown in Fig. 22. In this case, the assembly was done by hand which limits the achievable positioning accuracy. For commercial applications, more sophisticated methods of alignment and assembly should be used to ensure performance and repeatability. To improve the repeatability of the process and aid with the alignment, holders for each resonator were 3D-printed, shown in Fig. 23, for the glueing process. The quality factors of the post and the concentric-ring sample resonators were measured using the weak coupling method described in [27] and [28]. The measurements are sensitive to the alignment of the resonator with respect to the centre of the cavity, with a slight misalignment influencing the quality factor. A second consideration is that with a misalignment, a perturbation is caused in the field and the second orthogonal mode is coupled into as well, this will also affect the achieved quality factor of the measured resonance. The glue used to fix the resonators was standard off-the-shelf superglue and so introduces loss. The measured results of the Q-factor analysis

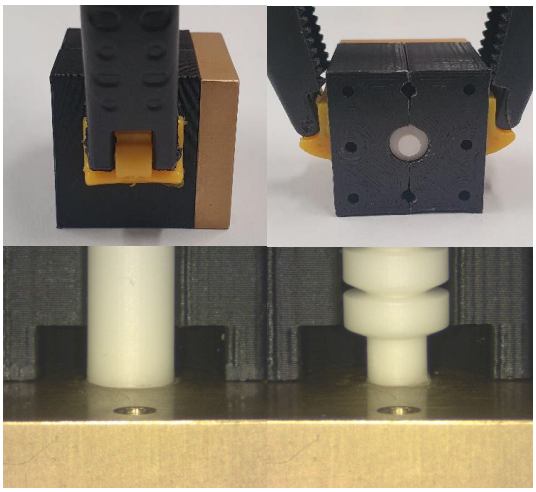

FIGURE 23. Two part 3D-printed resonator alignment holder, with the post on the left and the concentric ring resonator on the right.

are given in Fig. 24. Ten samples of each resonator were measured. An average value for the post was found to be approximately $Q_u = 4955$ and $Q_u = 7125$ for the concentric-ring resonator. This difference on average is approximately 2171 which is around 44%. The maximum achieved quality factor for each was $Q_u = 5366$ and $Q_u = 7274$, respectively, with a difference of 1907. The measurements were then repeated for the concentric-ring resonator in the copper cavity with an average $Q_u = 11841$. These results represent the best values achieved throughout the measurements and assembly process. The measured results are consistently close to the simulated values with the concentric-ring resonator. The rings have the effect of reducing the current along the base of the resonator and thus the losses from the mounting method with glue have less of an influence on the measured values. This is not the case for the regular post which, along with slight misalignment, helps explain the lower than predicted quality factor values. In the case of the post-type resonator, more sophisticated methods of mounting and lower loss/conductive adhesives could be attempted to improve the performance, this however would still be lower than that of the proposed concentric-ring type resonator. For both resonators, future print iterations could be scaled using a new compensation ratio to provide a more accurate result and shift the frequency back closer to that of the simulated value.

B. TE_{112} MODE SINGLET MEASUREMENT

The measured performance of the post and concentric-ring resonator brass singlets is shown in Fig. 25. The frequency shift of the resonators can be attributed primarily to the above mentioned enlargement of around 120 μm and slight tilting of the resonator due to the manual assembly. The concentric ring resonator has a measured insertion loss of 0.42 dB with an estimated $Q_u \approx 5900$ compared to the simulated $Q_u \approx 6900$. The measured resonant frequency shifted downwards by 1.93%, and the zero shifted downwards by 1.47%.

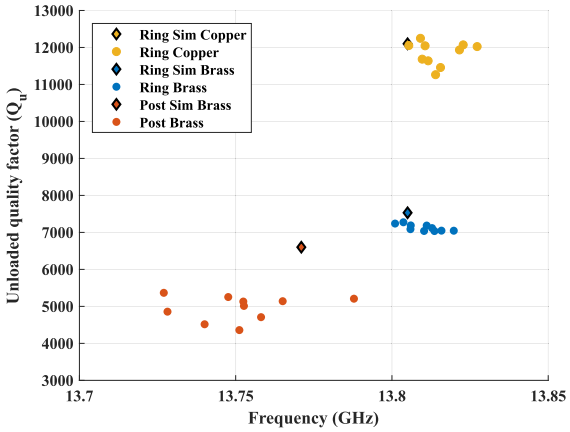

FIGURE 24. Measured quality factor of concentric-ring and post resonators in a CW614N cavity and concentric-ring resonators in a CW008A cavity.

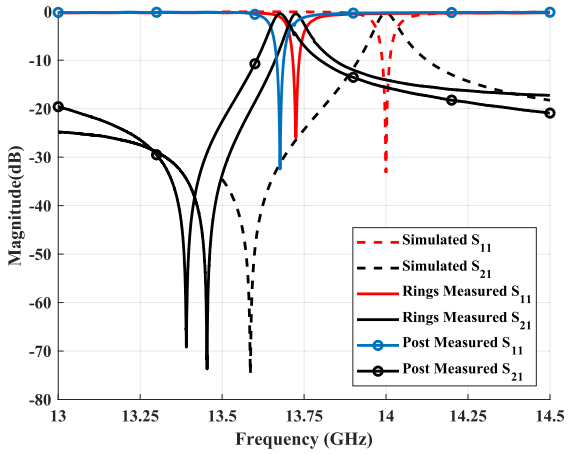

FIGURE 25. Measured singlet performance vs simulated design.

The uneven shifting of the pole and zero can be explained by slight tilting of the resonator during assembly, which changes the height of the probe feed slightly along the resonator compared to the design. Aside from the frequency shift, the results show good agreement with the simulated values.

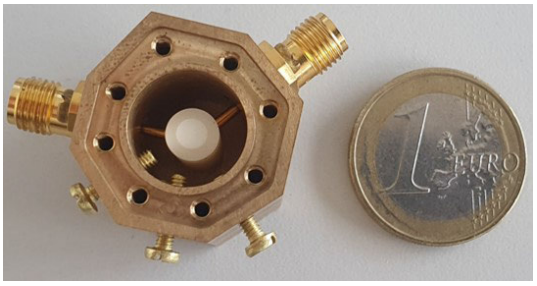

FIGURE 26. Fabricated TE_{112} dual-mode doublet.

C. TE_{112} DUAL-MODE DOUBLET MEASUREMENT

The fabricated CW614N brass doublet is shown in Fig. 26, along with the measured performance in Fig. 27.

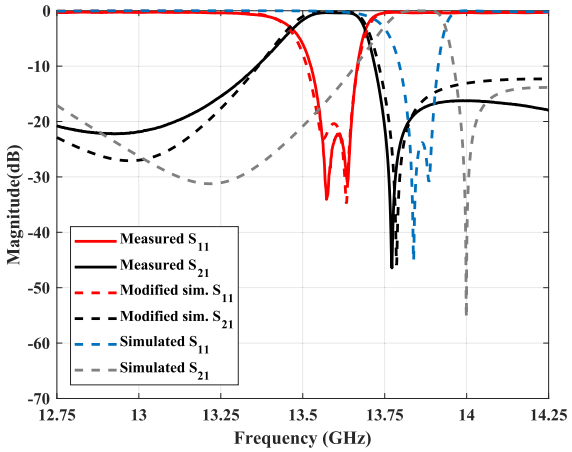

FIGURE 27. Measured doublet performance vs modified and design simulation.

The response has shifted downward in frequency by 1.43%, which is primarily attributed to the increase in resonator size and the use of glue. This hypothesis was confirmed by increasing the resonator size and adding a thin layer (70 μm) of glue ($\varepsilon_r = 3.3$) between the base of the resonator and the cavity in the simulations. The modified simulation results are also shown in Fig. 27 and align well with the measurements. The tuning screws of the fabricated filter allowed for most of the response to be recovered, however, a shift in the transmission zero shift below the passband and the degraded quality factor performance remain. The quality factor of the filter was calculated to be approximately 1800 compared to a simulated 3700, with an insertion loss of less than 0.39 dB and a return loss that averages 20 dB throughout the passband.

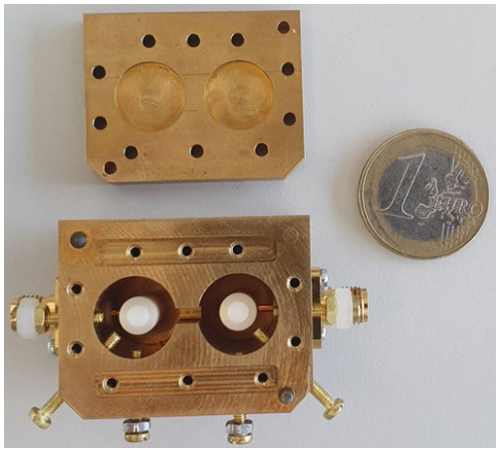

FIGURE 28. Fabricated TE_{112} dual-mode fourth-order filter.

D. TE_{112} DUAL-MODE FOURTH-ORDER FILTER

The assembled CW614N brass dual-mode filter is shown in Fig. 28, which was measured for two different zero positions.

TABLE 2. Comparison of 3D-printed dielectric filters in literature (where f_0 is center frequency, TZ is transmission zero, λ_0 is wavelength at the centre frequency and Q_u is the unloaded quality factor).

Ref.	f_0 (GHz)	Mode	Configuration	Order	TZ	Volume/λ_0^3	Q_u(*Simulated)
2017 [12]	11.76	$TE_{01\delta}$	Single mode	Sixth	2	$2.5 \times 2.07 \times 0.71$	1000
2022 [13]	8.3	$TM_{01\delta}$	Single mode	Second	0	$0.67 \times 0.24 \times 0.25$	600
2018 [15]	6	TM_{010}	Dual mode	Fourth	4	$0.68 \times 1.34 \times 0.28$	840
2022 [31]	6.1	TM_{010}	Single mode	Fourth	0	$1.16 \times 0.57 \times 0.57$(excluding housing)	1000
2022 [32]	14.125	$TE_{01\delta}/TE_{101}$	Dual mode	Fourth	3	$1.43 \times 0.9 \times 0.45$(excluding housing)	5600* /4000
2022 [33]	6.3	$TM_{01\delta}$	Single mode	Fourth	2	$1 \times 1.05 \times 0.86$	2000*/700
This work (doublet)	13.8	TE_{112}	Dual mode	Second	2	$0.55 \times 0.96 \times 0.55$ (excluding housing)	3700*/1800
This work (dual mode)	14	TE_{112}	Dual mode	Fourth	2	$1.28 \times 0.97 \times 0.56$ (excluding housing)	5600*/1100

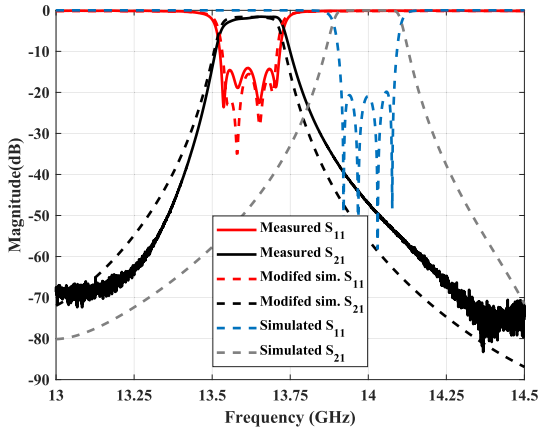

FIGURE 29. Measured dual-mode filter with first zero configuration performance vs modified and design simulations.

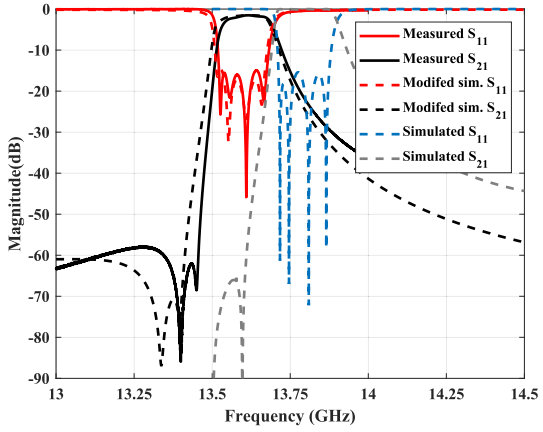

FIGURE 30. Measured dual-mode filter with second zero configuration performance vs modified and design simulations.

The measured performance with the dual-mode coupling screws at the height of 17.7 mm is shown in Fig. 29 and the second in the same filter with the coupling screws mirrored around the centre to the floor at 5.2 mm in Fig. 30. This demonstrates zero configurations on either side or both below the passband within the same design. It was not possible to fully recover the response due to the asymmetry and misalignment of the resonators. Each resonator position is also not identical to the other, with shift or angular misalignment being different in each. The tilting strongly affects the input coupling between the modes and differs at the two ports due to the manual assembly. The performance is thus degraded without additional means of recovery. Similar to the doublet case, modified simulations were performed for each filter to confirm the cause of the frequency shift. Again the resonator size was increased to match the fabricated dimensions, and a 70 μm layer of glue was added to the simulation. For the first configuration, it was also necessary to include a resonator tilt of 2° to model the shift in transmission zeros more closely. In both cases, an effective conductivity of 0.6 MS/m was simulated to approximate the increased losses of the prototypes. These modified simulations are also included in Fig. 29 and Fig. 30, respectively. The filters achieved an insertion loss of less than 2.08 dB and a return loss that averages 14 dB throughout the passband, and quality factors of 1100, compared to a simulated 5600. The filter response was shifted downwards by 2.66% for the first zeros configuration and 1.3% for the second.

The quality factor for all the prototypes fabricated, especially in the dual mode cases, experienced degradation compared to the simulated values. These prototypes were designed and manufactured for verification of the core concept of this work. They were all assembled by hand, in a simple manner, by the author. The most significant contributing factor to the reduction in quality factor is the accurate alignment and placement of each of the resonators inside the cavities, which is the case for dielectric resonators generally. The tuning screws present in the design could not wholly compensate for these assembly defects, thus making complete recovery of the filter response and associated quality factors impossible. Additionally, the tuning screws are made of brass, which contributes to a further reduction in the achievable quality factor. For future work, more sophisticated assembly methods would significantly improve the measured performance of the prototypes. Table 2 provides a comparison of this work with other recent works on 3D-printed dielectric filters.

VI. CONCLUSION

A novel 3D-printed resonator structure with concentric rings around a dielectric post resonator has been proposed to increase the quality factor performance. The rings enable an improved performance by moving the TE_{112} mode fields inside the cavity upwards and away from the cavity

floor and thereby reducing conductive losses. The novel concentric-ring resonator was measured and compared to a standard post at the same resonant frequency. The ten samples measured showed an average increase in the unloaded quality factor of 2171, or approximately 44%, successfully validating the design. The resonator was demonstrated in a singlet configuration with easily controllable zero positioning. Additionally, a doublet configuration was presented, successfully fabricated and measured. The doublet was extended into successfully demonstrating a dual-mode fourth-order filter with two transmission zeros in two configurations. The causes for frequency shift and performance degradation in the prototypes were also identified and validated through simulations. This work proves the design concept and highlights the potential of 3D-printed resonators to greatly improve the loss performance.

ACKNOWLEDGMENT

The authors thank Dominik Brouczek, Dr. Martin Schwentenwein, Lithoz, and the EBS Laboratory, TU Graz, for providing the equipment, materials and valuable technical experience enabling the work detailed in this paper.

REFERENCES

[1] I. C. Hunter, L. Billonet, B. Jarry, and P. Guillon, "Microwave filters-applications and technology," *IEEE Trans. Microw. Theory Techn.*, vol. 50, no. 3, pp. 794–805, Mar. 2002, doi: 10.1109/22.989963.

[2] R. J. Cameron, C. M. Kudsia, and R. R. Mansour, *Microwave Filters for Communication Systems: Fundamentals, Design, and Applications*. Hoboken, NJ, USA: Wiley, 2018.

[3] V. Nocella, L. Pelliccia, C. Tomassoni, and R. Sorrentino, "Miniaturized dual-band waveguide filter using TM dielectric-loaded dual-mode cavities," *IEEE Microw. Wireless Compon. Lett.*, vol. 26, no. 5, pp. 310–312, May 2016, doi: 10.1109/LMWC.2016.2549181.

[4] P. Vallerotonda, F. Cacciamani, L. Pelliccia, F. Aquino, C. Tomassoni, P. Martìn-Iglesias, and V. T. di Crestvolant, "Dielectric-loaded Ku-band filter for high-power space applications based on barrel-shaped cavities," in *Proc. 51st Eur. Microw. Conf. (EuMC)*, Apr. 2022, pp. 35–38.

[5] P. Vallerotonda, F. Cacciamani, L. Pelliccia, A. Cazzorla, D. Tiradossi, W. Steffè, F. Vitulli, E. Picchione, J. Galdeano, P. Martìn-Iglesias, and C. Tomassoni, "Dielectric-loaded L-band filters for high-power space applications," *Int. J. Microwave and Wireless Technol.*, vol. 14, no. 3, pp. 1–11, 2022.

[6] G. Shen and D. Budimir, "Novel resonator structures for combline filter applications," in *Proc. 32nd Eur. Microw. Conf.*, Oct. 2002, pp. 1–3, doi: 10.1109/EUMA.2002.339355.

[7] M. Hoft, T. Magath, O. Bartz, and S. Burger, "Corner rounding for increased quality factor of cavity resonators," in *Proc. Asia–Pacific Microw. Conf.*, 2005, p. 4, doi: 10.1109/APMC.2005.1606272.

[8] C. Wang and K. A. Zaki, "Dielectric resonators and filters," *IEEE Microw. Mag.*, vol. 8, no. 5, pp. 115–127, Oct. 2007, doi: 10.1109/MMM.2007.903648.

[9] R. R. Mansour, "High-Q tunable dielectric resonator filters," *IEEE Microw. Mag.*, vol. 10, no. 6, pp. 84–98, Oct. 2009.

[10] J. Krupka, M. E. Tobar, J. G. Hartnett, D. Cros, and J. M. L. Floch, "Extremely high-Q factor dielectric resonators for millimeter-wave applications," *IEEE Trans. Microw. Theory Techn.*, vol. 53, no. 2, pp. 702–712, Feb. 2005, doi: 10.1109/TMTT.2004.840572.

[11] A. Panariello, M. Yu, and C. Ernst, "Ku-band high power dielectric resonator filters," *IEEE Trans. Microw. Theory Techn.*, vol. 61, no. 1, pp. 382–392, Jan. 2013, doi: 10.1109/TMTT.2012.2229292.

[12] A. Perigaud, O. Tantot, N. Delhote, S. Verdeyme, S. Bila, and D. Baillargeat, "Bandpass filter based on skeleton-like monobloc dielectric pucks made by additive manufacturing," in *Proc. 48th Eur. Microw. Conf. (EuMC)*, Sep. 2018, pp. 296–299, doi: 10.23919/EuMC.2018.8541710.

[13] C. Carceller, F. Gentili, D. Reichartzeder, W. Bosch, and M. Schwentenwein, "Practical considerations in the design of monoblock TM dielectric resonator filters with additive manufacturing," in *Proc. Int. Conf. Electromagn. Adv. Appl. (ICEAA)*, Sep. 2017, pp. 364–367, doi: 10.1109/ICEAA.2017.8065251.

[14] C. Carceller, F. Gentili, W. Bosch, D. Reichartzeder, and M. Schwentenwein, "Ceramic additive manufacturing as an alternative for the development of miniaturized microwave filters," in *IEEE MTT-S Int. Microw. Symp. Dig.*, Sep. 2017, pp. 1–3, doi: 10.1109/IMWS-AMP.2017.8247373.

[15] D. Miek, M. Hoft, J. A. Lorente, A. Berger, D. Brouczek, M. Schwentenwein, A. Brandao, P. Martin-Iglesias, and V. T. D. Crestvolant, "Ceramic additive manufactured monolithic X-shaped TM dual-mode filter," *IEEE J. Microw.*, vol. 2, no. 3, pp. 496–506, Jul. 2022, doi: 10.1109/JMW.2022.3167250.

[16] L. Robins, A. Arsanjani, C. Bartlett, R. Teschl, W. Bosch, and M. Hoft, "Additive manufacturing of non-homogenous dielectric waveguide structures and filters," in *IEEE MTT-S Int. Microw. Symp. Dig.*, Nov. 2021, pp. 326–328, doi: 10.1109/IMFW49589.2021.9642291.

[17] Lithoz. *Materialübersicht LCM-Technologie*. Accessed: Jul. 21, 2022. [Online]. Available: https://lithoz.com/wp-content/uploads/2022/04/LITHOZ_Materialfolder_DE_web.pdf

[18] M. Schwentenwein, P. Schneider, and J. Homa, "Lithography-based ceramic manufacturing: A novel technique for additive manufacturing of high-performance ceramics," in *Advances in Science and Technology*, vol. 88. Wollerau, Switzerland: Trans Tech, 2014, pp. 60–64.

[19] S. Amari, U. Rosenberg, and J. Bornemann, "Singlets, cascaded singlets, and the nonresonating node model for advanced modular design of elliptic filters," *IEEE Microw. Wireless Compon. Lett.*, vol. 14, no. 5, pp. 237–239, Mar. 2004, doi: 10.1109/LMWC.2004.827866.

[20] S. Bastioli, "Nonresonating mode waveguide filters," *IEEE Microw. Mag.*, vol. 12, no. 6, pp. 77–86, Oct. 2011, doi: 10.1109/MMM.2011.942009.

[21] S. Amari and U. Rosenberg, "Characteristics of cross (bypass) coupling through higher/lower order modes and their applications in elliptic filter design," *IEEE Trans. Microw. Theory Techn.*, vol. 53, no. 10, pp. 3135–3141, Oct. 2005, doi: 10.1109/TMTT.2005.855359.

[22] Y. Xiao, P. Shan, K. Zhu, H. Sun, and F. Yang, "Analysis of a novel singlet and its application in THz bandpass filter design," *IEEE Trans. THz Sci. Technol.*, vol. 8, no. 3, pp. 312–320, May 2018, doi: 10.1109/TTHZ.2018.2823541.

[23] S. Amari and U. Rosenberg, "The doublet: A new building block for modular design of elliptic filters," in *Proc. 32nd Eur. Microw. Conf.*, Oct. 2002, pp. 1–3, doi: 10.1109/EUMA.2002.339308.

[24] S. Amari, "On the theory and modeling of dual-mode cavity microwave bandpass filters," in *IEEE MTT-S Int. Microw. Symp. Dig.*, Jun. 2012, pp. 1–3, doi: 10.1109/MWSYM.2012.6259600.

[25] S. J. Fiedziuszko, "Dual-mode dielectric resonator loaded cavity filters," *IEEE Trans. Microw. Theory Techn.*, vol. MTT-30, no. 9, pp. 1311–1316, Sep. 1982.

[26] G. Bianchi and R. Sorrentino, *Electronic Filter Simulation & Design*. New York, NY, USA: McGraw-Hill Professional, 2007.

[27] L. F. Chen, C. K. Ong, C. P. Neo, V. V. Varadan, and V. K. Varadan, *Microwave Electronics Measurement and Materials Characterisation*. Hoboken, NJ, USA: Wiley, 2004.

[28] J.-S. Hong and M. J. Lancaster, *Microstrip Filters for RF/Microwave Applications*. New York, NY, USA: Wiley, 2001.

[29] Gemmel Metalle. *Legierungsbeschreibung CuZn39Pb3*. Accessed: Jul. 21, 2022. [Online]. Available: https://www.gemmel-metalle.de/informationen/datenblaetter.html#messing

[30] Gemmel Metalle. *Legierungsbeschreibung Cu-OF*. Accessed: Jul. 21, 2022. [Online]. Available: https://www.gemmel-metalle.de/informationen/datenblaetter.html#kupfer

[31] A. Widaa, F. Cacciamani, L. Pelliccia, C. Tomassoni, V. T. di Crestvolant, and M. Hoft, "Compact ultra-wideband bandpass filter using additively manufactured TM–mode dielectric resonators," in *Proc. 52nd Eur. Microw. Conf. (EuMC)*, Sep. 2022, pp. 115–118, doi: 10.23919/EuMC54642.2022.9924504.

[32] E. Lopez-Oliver, C. Tomassoni, F. Cacciamani, L. Pelliccia, and V. T. D. Crestvolant, "Bandpass filter based on 3-D-printed ceramic resonators," in *Proc. 24th Int. Microw. Radar Conf. (MIKON)*, Sep. 2022, pp. 1–5.

[33] P. Vallerotonda, F. Cacciamani, L. Pelliccia, C. Tomassoni, G. Cannone, and V. T. di Crestvolant, "Compact ultra-wideband cavity filter based on suspended ceramic resonators in additive manufacturing," in *IEEE MTT-S Int. Microw. Symp. Dig.*, Jun. 2022, pp. 92–95, doi: 10.1109/IMS37962.2022.9865629.

LUKE ROBINS (Member, IEEE) was born in Surrey, U.K., in 1989. He received the B.Eng. degree in electrical and electronic engineering from Stellenbosch University, South Africa, in 2013, and the M.Eng. degree (Hons.) in telecommunications engineering from the University of Witwatersrand, Johannesburg, South Africa, in 2017. He is currently pursuing the Dr.Techn. degree with the Graz University of Technology, Graz, Austria. From 2014 to 2017, he completed his Engineer-in-Training Program at Eskom, the South African National Power Utility, gaining experience with power generation, control and instrumentation, renewable energy, and smart grids. From 2017 to 2019, he worked as a Project Manager with Huawei on South African national telecommunications infrastructure projects. He was then awarded a Fellowship as part of the Tesla Project (811232-H2020-MSCA-ITN-2018) and worked as an Early Stage Researcher, during 2019–2022. He is currently employed as a Systems Project Manager with Infineon Technologies, Graz, Austria. His research interests include additive manufacturing, dielectric resonators, passive RF component design, and RF filters.

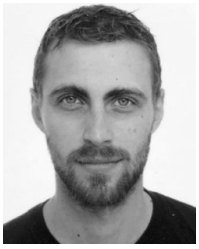

CHAD BARTLETT (Graduate Student Member, IEEE) was born in Nelson, BC, Canada, in 1987. He received the B.Eng. and M.A.Sc. degrees in electrical engineering from the University of Victoria, Victoria, BC, Canada, in 2017 and 2019, respectively. He is currently pursuing the Dr.-Ing. degree with the Chair of Microwave Engineering, Institute of Electrical Engineering and Information Engineering, University of Kiel, Kiel, Germany. His research interests include microwave and millimeter-wave passive components, filters, and antenna networks for the next generation of satellite and communication systems, as well as developing methods for overcoming challenges in micro-scale designs. He is a member of the European Union's Horizon 2020 Research and Innovation Program for Early-Stage Researchers.

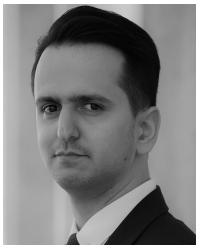

ARASH ARSANJANI (Member, IEEE) was born in Kerman, Iran, in 1992. He received the B.Sc. degree in electrical engineering from the Shahid Bahonar University of Kerman, Kerman, in 2015, and the M.Sc. degree in electrical engineering from the K. N. Toosi University of Technology, Tehran, Iran, in 2018. He is currently pursuing the Ph.D. degree with the Graz University of Technology, Graz, Austria. His current field of study as a part of European Union's Horizon 2020 Research and Innovation Program includes low-loss microwave components for satellite applications. His research interests include microwave and mm-wave filter and antenna design, metamaterial, and metasurfaces.

ABDULRAHMAN WIDAA (Graduate Student Member, IEEE) was born in Wad Medani, Gezira, Sudan, in 1991. He received the B.Sc. degree (Hons.) in telecommunication engineering from the University of Gezira, Wad Madani, in 2014, and the M.Eng. degree in information and communication engineering from the University of Electronic Science and Technology of China, Chengdu, China, in 2018. He is currently pursuing the Dr.-Ing. degree in electrical and information engineering with the University of Kiel, Kiel, Germany.

From 2014 to 2016, he was a Teaching Assistant with the Electronics Engineering Department, University of Gezira. From 2016 to 2018, he was a Research Assistant with the University of Electronic Science and Technology of China, where he was involved in the design of tunable filters for RF/microwave applications. From 2018 to 2019, he was a Lecturer with the Electronics Engineering Department, University of Gezira. Since 2019, he has been a Researcher with the Chair of Microwave Engineering, University of Kiel, under the European Union's Project of Advanced Technologies for future European Satellite Applications (TESLA). He was a Visiting Researcher with the Technische Universität Darmstadt, Darmstadt, Germany, from February 2020 to March 2020; the University of Perugia, Perugia, Italy; RF Microtech S.r.l, Perugia, from May 2021 to July 2021; and the Universitat Politècnica de València, Valencia, Spain, from April 2022 to May 2022. His research interests include design of miniaturized/tunable filters and components for microwave and satellite communications, sensors, and embedded systems.

Mr. Widaa was a recipient of many national and international awards, scholarships, and grants, including the Chinese University Master Scholarship Program, in 2016, and the European Microwave Week Student Grant, in 2020 and 2021.

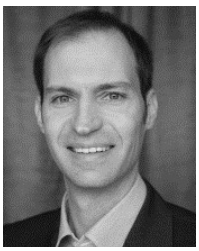

REINHARD TESCHL (Member, IEEE) was born in Graz, Austria. He received the master's and Ph.D. degrees in information and computer engineering from the Graz University of Technology (TU Graz), in 2001 and 2010, respectively. From 2010 to 2017, he was a Senior Scientist at the Radar and Microwave Propagation Group, Institute of Microwave and Photonic Engineering (IHF), TU Graz, where he worked on weather radar systems and conducted data-based atmospheric- and hydrological studies. Since 2017, he has been a University Assistant at IHF, teaching courses on communication engineering, antennas and RF/microwave component design. He is currently a Project Leader with the IHF Research Group on antennas and filters and an Associate Researcher at the TU Graz Research Centre 'Dependable Internet of Things in Adverse Environments.' His research interests include adaptable passive microwave components and related manufacturing challenges. He is acting as a Reviewer for IEEE TRANSACTIONS ON MICROWAVE THEORY AND TECHNIQUES and *EuMA International Journal of Microwave and Wireless Technologies* and is involved in the organization of IEEE co-sponsored scientific conferences (Organizing Committee Co-Chair: CoBCom 2020 & 2022, ConTEL 2019 & 2023).

MICHAEL HÖFT (Senior Member, IEEE) was born in Lübeck, Germany, in 1972. He received the Dipl.-Ing. and Dr.-Ing. degrees in electrical engineering from the Hamburg University of Technology, Hamburg, Germany, in 1997 and 2002, respectively. From 2002 to 2013, he was with the Communications Laboratory, European Technology Center, Panasonic Industrial Devices Europe GmbH, Lüneburg. He was a Research Engineer and then the Team Leader, where he had been engaged in research and development of microwave circuitry and components, particularly filters for cellular radio communications. From 2010 to 2013, he was the Group Leader of research and development of sensor and network devices. Since October 2013, he has been a Full Professor with the Faculty of Engineering, University of Kiel, Kiel, Germany, where he is currently the Head of the Microwave Group, Institute of Electrical and Information Engineering. His research interests include active and passive microwave components, submillimeter-wave quasioptical techniques and circuitry, microwave and field measurement techniques, microwave filters, microwave sensors, and magnetic field sensors. He is a member of the European Microwave Association (EuMA), the Association of German Engineers (VDI), and the German Institute of Electrical Engineers (VDE).

WOLFGANG BÖSCH (Fellow, IEEE) received the Dipl.Ing. degree from the Technical University of Vienna, Vienna, Austria, in 1985, the Ph.D. degree from the Graz University of Technology, Graz, Austria, in 1988, and the M.B.A. degree from the School of Management, University of Bradford, Bradford, U.K., in 2004. He joined the Graz University of Technology to establish a new Institute for Microwave and Photonic Engineering. His institute has more than 45 researchers, on average 60 publications per year and a research project turnover of €1.7 million per year. Previously, he was the Chief Technology Officer (CTO) of the Advanced Digital Institute, Shipley, U.K., a not-for-profit organization to promote research activities. Earlier, he worked as the Director of the Business and Technology Integration for RFMD, Reading, U.K., and for almost ten years, he has been with Filtronic plc, Yeadon, U.K., as a CTO of Filtronic Integrated Products and the Director of the Global Technology Group, New York, NY, USA. Before joining Filtronic, he held positions with the European Space Agency (ESA), Paris, France, working on amplifier linearization techniques, with MPR-Teltech, Burnaby, BC, Canada, working on MMIC technology projects, and with the Corporate Research and Development Group of M/A-COM, Boston, MA, USA, where he worked on advanced topologies for high-efficiency power amplifiers. For four years, he was with DaimlerChrysler Aerospace (now Airbus), Munich, Germany, working on T/R modules for airborne radar. He is currently the Dean of the Faculty of Electrical and Information Engineering, Graz University of Technology, which also incorporates 13 institutes and 18 full professors. He has published more than 150 articles and holds four patents. He is a fellow of the IET.